Eleventh International Conference on Computational Fluid Dynamics (ICCFD11), Maui, HI, USA, July 11-15, 2022

ICCFD11-2022-0402

Positivity-preserving Entropy Stable Spectral Collocation Schemes of Arbitrary Order of Accuracy for the 3-D Navier-Stokes Equations

N. K. Yamaleev[†] and J. Upperman[†,*]
Corresponding author: nyamalee@odu.edu

[†] Old Dominion University, USA.

Abstract: We have developed a new family of positivity-preserving, entropy stable spectral collocation schemes of arbitrary order of accuracy for the 3-D compressible Navier-Stokes equations on unstructured hexahedral grids. The proposed schemes are constructed by using a flux-limiting technique that combines a positivity-violating entropy stable method of arbitrary order of accuracy and a novel first-order positivity-preserving entropy stable finite volume-type scheme, which are both discretized on the same Legendre-Gauss-Lobatto grids. To provide the positivity preservation and excellent discontinuity-capturing properties, the Navier-Stokes equations are regularized by adding artificial dissipation in the form of the Brenner-Navier-Stokes diffusion operator. The resultant scheme is conservative, design-order accurate for smooth solutions, and pointwise positivity preserving. To our knowledge, this is the first family of schemes of arbitrary order of accuracy that provably guarantee both pointwise positivity of thermodynamic variables and L_2 stability for the 3-D compressible Navier-Stokes equations. Numerical results demonstrating accuracy and positivity-preserving properties of the new schemes are presented for viscous flows with nearly vacuum regions and very strong shocks and contact discontinuities.

Keywords: Summation-by-parts (SBP) operators, Entropy stability, Spectral collocation schemes, Positivity-preserving methods, Brenner-Navier-Stokes equations, Artificial dissipation.

1 Introduction

Global positivity of thermodynamic variables (e.g., density and temperature) is a necessary condition for hyperbolicity of the Euler equations and existence of entropy solutions of the compressible Navier-Stokes equations. Therefore, the pointwise positivity of density and temperature is vital for constructing stable and robust numerical schemes for the compressible Euler and Navier-Stokes equations. Positivity-preserving methods available in the literature for the compressible Navier-Stokes equations are very rare and either limited to so-called weak positivity (which does not guarantee pointwise positivity of the thermodynamic variables) [1] or to at most 2nd-order schemes in space and time [2, 3]. To our knowledge, there are no high-order numerical schemes that provide both entropy stability and pointwise positivity of the thermodynamic variables for the 3-D compressible Navier-Stokes equations.

Herein, we generalize and extend the 1-D positivity-preserving entropy stable methodology developed in [4, 5] to the three-dimensional compressible Navier-Stokes equations on static unstructured hexahedral grids. Similar to the 1-D high-order schemes in [5], the new schemes for the 3-D compressible Navier-Stokes equations are constructed by combining a positivity-violating entropy stable method of arbitrary order of accuracy and a novel first-order positivity-preserving entropy stable method developed in [6]. The novel high-order schemes provide an arbitrary order of accuracy for sufficiently smooth solutions of the 3-D compressible Navier-Stokes equations and the pointwise positivity at individual collocation points that are directly used

[*] Current address: AFRL, Kirtland AFB, USA

for approximation of the governing equations. Another distinctive feature of the proposed methodology is that the new high-order positivity-preserving schemes satisfy the discrete entropy inequality, thus facilitating a rigorous L_2-stability proof for the symmetric form of the discretized Navier-Stokes equations [7]. To our knowledge, this is the first family of high-order schemes that are both pointwise positivity preserving and entropy stable for the 3-D compressible Navier-Stokes equations.

2 Regularized Navier-Stokes equations

There are no theoretical results showing that the compressible Navier-Stokes equations themselves guarantee positivity of the thermodynamic variables. To overcome this problem, we regularize the Navier-Stokes equations by adding artificial dissipation in the form of the diffusion operator of the Brenner-Navier-Stokes equations introduced in [8]. The Brenner-Navier-Stokes equations are given by

$$\frac{\partial \boldsymbol{U}}{\partial t} + \sum_{m=1}^{3} \frac{\partial \boldsymbol{F}_{x_m}}{\partial x_m} = \sum_{m=1}^{3} \frac{\partial \boldsymbol{F}^{(B)}_{x_m}}{\partial x_m}, \quad \forall\, (x_1, x_2, x_3) \in \Omega, \quad t \geq 0, \tag{1}$$

$$\boldsymbol{F}^{(B)}_{x_m} = \boldsymbol{F}^{(v)}_{x_m} + \sigma \frac{\partial \rho}{\partial x_m} \begin{bmatrix} 1 & \boldsymbol{V} & E \end{bmatrix}^{\top}, \tag{2}$$

where $\boldsymbol{U} = [\rho, \rho V_1, \rho V_2, \rho V_3, \rho E]^{\mathrm{T}}$ is a vector of the conservative variables, σ is the volume diffusivity, and $\boldsymbol{F}^{(v)}_{x_m}, m = 1, 2, 3$, are the Navier-Stokes viscous fluxes.

The Brenner-Navier-Stokes equations (1) possess some remarkable properties that are not available for the Navier-Stokes equations. Equations (1) guarantee existence of a weak solution and uniqueness of a strong solution if the latter exists, ensure global-in-time positivity of the thermodynamic variables, satisfy a large class of entropy inequalities, and is compatible with a minimum entropy principle [9, 10]. Capitalizing on these remarkable properties of the Brenner-Navier-Stokes equations, we regularize the Navier-Stokes equations as follows:

$$\frac{\partial \boldsymbol{U}}{\partial t} + \sum_{m=1}^{3} \frac{\partial \boldsymbol{F}_{x_m}}{\partial x_m} = \sum_{m=1}^{3} \left[\frac{\partial \boldsymbol{F}^{(v)}_{x_m}}{\partial x_m} + \frac{\partial \boldsymbol{F}^{(AD)}_{x_m}}{\partial x_m} \right], \tag{3}$$

where the the artificial dissipation flux $\boldsymbol{F}^{(AD)}_{x_m}$ can be obtained from the viscous flux of the Brenner-Navier-Stokes equations, $\boldsymbol{F}^{(B)}_{x_m}$, by setting $\mu = \mu^{AD}$, $\sigma = c_\rho \mu^{AD}/\rho$, and $\kappa = c_T \mu^{AD}$. The coefficient μ^{AD} is an artificial viscosity and c_T and c_ρ are positive tunable coefficients, which are set equal to $c_\rho = 0.9$ and $c_T = \frac{c_\rho}{\gamma - 1}$ for all test problems presented herein.

A necessary condition for selecting a unique, physically relevant solution among possibly many weak solutions of the compressible Navier-Stokes equations is the entropy inequality. Both the Navier-Stokes and regularized Navier-Stokes equations are equipped with the same convex scalar entropy function $\mathcal{S} = -\rho s$ and entropy flux $\mathcal{F} = -\rho s \boldsymbol{V}$, where s is the thermodynamic entropy. It can be shown that the following inequality holds for both the conventional and regularized Navier-Stokes equations assuming the corresponding boundary conditions are entropy stable (e.g., see [11]):

$$\int_{\hat{\Omega}} \frac{\partial (J\mathcal{S})}{\partial \tau} \mathrm{d}\hat{\Omega} = \frac{d}{d\tau} \int_{\hat{\Omega}} J\mathcal{S} \mathrm{d}\hat{\Omega} \leq 0. \tag{4}$$

Along with the entropy inequality given by Eq. (4), the regularized Navier-Stokes equations (Eq. (3)) preserve some other key properties of the Brenner-Navier-Stokes equations including the positivity of thermodynamic variables. Herein, we present novel high-order schemes that mimic these properties of the 3-D regularized Navier-Stokes equations at the discrete level.

3 Summation-by-parts operators

The derivatives in Eq. (3) are discretized by spectral collocation operators that satisfy the summation-by-parts (SBP) property [12]. In one spatial dimension, this mimetic property is achieved by approximating

the first derivative with a discrete operator, D, as follow:

$$\begin{aligned} &D = \mathcal{P}^{-1}\mathcal{Q}, \quad \mathcal{P} = \mathcal{P}^\top, \quad \mathbf{v}^\top \mathcal{P}\mathbf{v} > 0, \quad \forall \mathbf{v} \neq \mathbf{0}, \\ &\mathcal{Q} = B - \mathcal{Q}^\top, \quad B = \mathrm{diag}(-1, 0, \ldots, 0, 1), \end{aligned} \tag{5}$$

where $\mathcal{P}$ and $\mathcal{Q}$ are local mass and stiffness matrices, respectively. Only diagonal-norm SBP operators are considered herein, which are used for proving the entropy inequality at the semi-discrete level [12].

In one spatial dimension, the physical domain is divided into K non-overlapping elements $[x_1^k, x_{N_p}^k]$, so that $x_1^k = x_{N_p}^{(k-1)}$. The discrete solution inside each element is defined on Legendre-Gauss-Lobatto (LGL) points, $\mathbf{x}_k = \left[x_1^k, \ldots, x_{N_p}^k\right]^\top$. These local points $\mathbf{x}_k$ are referred to as solution points. Along with the solution points, we also define a set of intermediate points $\bar{\mathbf{x}}_k = \left[\bar{x}_0^k, \ldots, \bar{x}_{N_p}^k\right]^\top$ prescribing bounding control volumes around each solution point. These points referred to as flux points form a complementary grid whose spacing is precisely equal to the diagonal elements of the positive definite matrix $\mathcal{P}$ in Eq. (5), i.e., $\Delta\bar{\mathbf{x}} = \mathcal{P}\mathbf{1}$, where $\bar{\mathbf{x}} = \left[\bar{x}_0, \ldots, \bar{x}_{N_p}\right]^\top$ is a vector of flux points, $\mathbf{1} = [1, \ldots, 1]^\top$, and Δ is an $N_p \times (N_p + 1)$ matrix corresponding to the two-point backward difference operator [12, 13]. As has been proven in [14], these discrete SBP derivative operators can be recast in the following telescopic flux form:

$$\mathcal{P}^{-1}\mathcal{Q}\mathbf{f} = \mathcal{P}^{-1}\Delta\bar{\mathbf{f}}, \tag{6}$$

where $\bar{\mathbf{f}}$ is a pth-order flux vector defined at the flux points. These 1-D SBP operators can be directly extended to three spatial dimensions via the tensor product arithmetic [15].

4 High-order positivity-violating entropy stable schemes

With the 3-D SBP operators discussed in the previous section, a baseline 3-D p^{th}-order semi-discrete spectral collocation scheme for the regularized 3-D Navier-Stokes equations (1) can be written as follows:

$$\left(\hat{\mathbf{U}}_p\right)_t + \sum_{l=1}^{3} \mathcal{P}_{\xi^l}^{-1} \Delta_{\xi^l} \hat{\bar{\mathbf{f}}}_l^p - D_{\xi^l}\left[\hat{\mathbf{f}}_l^{p(v)} + \hat{\mathbf{f}}_l^{p(AD)}\right] = \sum_{l=1}^{3} \mathcal{P}_{\xi^l}^{-1}\left[\hat{\mathbf{g}}_l^{p(AD)} + \hat{\mathbf{g}}_l\right], \tag{7}$$

where $\hat{\mathbf{U}}_p = [J]\,\mathbf{U}_p$, $\hat{\mathbf{g}}_l$ is boundary and interface penalty terms.

The p^{th}-order contravariant inviscid fluxes, $\hat{\bar{\mathbf{f}}}_l^p$, defined at flux points are given by

$$\begin{aligned} \hat{\bar{\mathbf{f}}}_m^p(\vec{\xi}_{\bar{i}}) &= \sum_{j=i+1}^{N} \sum_{l=1}^{i} 2 q_{l,j} \bar{f}_{(S)}(\mathbf{U}_p(\vec{\xi}_l), \mathbf{U}_p(\vec{\xi}_j)) \tfrac{\hat{\mathbf{a}}^m(\vec{\xi}_l) + \hat{\mathbf{a}}^m(\vec{\xi}_j)}{2} \text{ for } 1 \leq i \leq N-1, \\ \hat{\bar{\mathbf{f}}}_m^p(\vec{\xi}_{\bar{i}}) &= \bar{f}_{(S)}(\mathbf{U}_p(\vec{\xi}_{\bar{i}}), \mathbf{U}_p(\vec{\xi}_{\bar{i}}))\hat{\mathbf{a}}^m(\vec{\xi}_{\bar{i}}) \text{ for } \bar{i} \in \{0, N\}, \end{aligned} \tag{8}$$

where $m = 1, 2, 3$ and $\bar{f}_{(S)}(\cdot, \cdot)$ is a two-point, consistent, entropy conservative flux that satisfies

$$(w_1 - w_2)^\top \bar{f}_{(S)}(U_1, U_2) = \vec{\psi}_1 - \vec{\psi}_2 \tag{9}$$

for any two admissible states U_1 and U_2 [16]. For all test problems considered, we use the entropy conservative flux developed in [17]. In [6], we show that the proposed method for ensuring positivity is independent of a particular choice of $\bar{f}_{(S)}$. In the above equation and hereafter, $\hat{\mathbf{a}}_m^l(\vec{\xi}_{ijk})$ is a pth-order discrete approximation of $J\frac{\partial \xi^l}{\partial x^m}$ at the solution point $\vec{\xi}_{ijk}$, which is constructed such that it satisfied the geometric conservation law (GCL) equations (e.g., see [18]). The high-order contravariant viscous and artificial dissipation fluxes, $\hat{\mathbf{f}}_l^{(v)}$, are constructed as follows:

$$\hat{\mathbf{f}}_l^{p(vis)} = \sum_{m=1}^{3} [\hat{a}_m^l] \mathbf{f}_{x^m}^{p(vis)}, \quad \mathbf{f}_{x^m}^{p(vis)} = \sum_{j=1}^{3} [c_{m,j}^{(vis)}] \mathbf{\Theta}_{x^j}, \tag{10}$$

where $\hat{\mathbf{f}}_l^{p(vis)} = \hat{\mathbf{f}}_l^{p(v)}$ or $\hat{\mathbf{f}}_l^{p(vis)} = \hat{\mathbf{f}}_l^{p(AD)}$ and $[c_{m,j}^{(vis)}], 1 \leq m, j \leq 3$ are the corresponding viscosity matrices. For each $1 \leq m, j \leq 3$, $[c_{m,j}^{(vis)}]$ is a block-diagonal matrix with 5×5 blocks, such that $[\left(c_{m,j}^{(vis)}\right)^T] = [c_{j,m}^{(vis)}]$, and $\sum_{m=1}^{3}\sum_{j=1}^{3} \mathbf{v}^T[c_{m,j}^{(vis)}]\mathbf{v} \geq 0, \forall \mathbf{v}$, i.e., the full viscous/artificial dissipation tensor is symmetric positive semi-definite (SPSD). The gradient of the entropy variables, $\mathbf{\Theta}_{x^j}$, is discretized by using an approach that closely resembles the local discontinuous Galerkin (LDG) method developed in [19].

The high-order spectral collocation scheme given by Eq. (7) is conservative and stable in the entropy sense. The conservation follows immediately from the telescopic flux form of the inviscid terms and the SBP form of the viscous and artificial dissipation terms. The entropy stability of the discretized Navier-Stokes terms in Eq. (7) is proven in [12]. The entropy dissipation properties of the artificial dissipation terms follow immediately form Eq. (10) and the symmetric positive semi-definiteness of the artificial viscous tensor $[c_{m,j}^{(B)}]$, $1 \leq m, j \leq 3$. Note, however, that entropy stability alone does not guarantee the positivity of thermodynamic variables, if strong discontinuities are present in the domain. To address this limitation of the high-order schemes, we develop a novel first-order positivity-preserving entropy stable scheme for the 3-D Navier-Stokes equations, which is presented next.

5 First-order positivity-preserving entropy stable scheme

5.1 First-order scheme

For each high-order element, the first-order scheme is approximated on the same LGL points used for the high-order scheme. The first-order scheme treats solution points in a finite volume manner with the flux points acting as control volume edges and can be written as

$$\left(\hat{\mathbf{U}}_1\right)_t + \sum_{l=1}^{3} \mathcal{P}_{\xi^l}^{-1} \Delta_{\xi^l} \left[\hat{\tilde{\mathbf{f}}}_l^1 - \hat{\tilde{\mathbf{f}}}_{\hat{\sigma},l}^{1(AD)} - \hat{\tilde{\mathbf{f}}}_l^{1(AD)}\right] - D_{\xi^l}\hat{\mathbf{f}}_l^{p(v)} = \sum_{l=1}^{3} \mathcal{P}_{\xi^l}^{-1} \left[\hat{\mathbf{g}}_l + \hat{\mathbf{g}}_l^{1(AD)}\right], \tag{11}$$

where $\hat{\tilde{\mathbf{f}}}_l^1$ and $\hat{\tilde{\mathbf{f}}}_{\hat{\sigma},l}^{1(AD)}$, $\hat{\tilde{\mathbf{f}}}_l^{1(AD)}$ are first-order inviscid and artificial dissipation fluxes, $\hat{\mathbf{f}}_l^{p(v)}, l = 1, 2, 3$, are the high-order physical fluxes, and $\hat{\mathbf{g}}_l$ are inviscid and viscous penalties that are identical to those used in [12].

Note that the discretization of the first-order inviscid fluxes on high-order LGL elements requires special care. In [20, 21], it was suggested to approximate the first-order inviscid fluxes at each flux point by using the arithmetic average of the metric coefficients associates with this subcell interface (see Eq. (B52) in [21]). One of the major pitfalls of this approach is that this approximation is neither freestream–preserving for constant flows nor entropy conservative for isentropic flows. Thus, the corresponding scheme does not satisfy the geometric conservation laws and over dissipates the numerical solution in regions where the entropy dissipation is not needed.

To overcome this problem, we discretize the inviscid fluxes in Eq. (11) by using an approximation introduced in [6, 22]. These inviscid fluxes are represented as the sum of entropy conservative and entropy dissipative terms: $\hat{\tilde{\mathbf{f}}}_l^1 = \hat{\tilde{\mathbf{f}}}_l^{(EC)} - \hat{\tilde{\mathbf{f}}}_l^{(ED)}$, where $\hat{\tilde{\mathbf{f}}}_l^{(ED)}$ is an entropy dissipative characteristic flux developed in [23], which is approximated so that it facilitates the pointwise density positivity [6]. The entropy conservative flux, $\hat{\tilde{\mathbf{f}}}_l^{(EC)}$, is discretized as follows:

$$\begin{cases} \hat{\tilde{\mathbf{f}}}^{(EC)}(\vec{\xi}_{\bar{i}}) = \bar{f}_{(S)}(\mathbf{U}_1(\vec{\xi}_i), \mathbf{U}_1(\vec{\xi}_{i+1}))\hat{\tilde{\vec{\mathbf{a}}}}^1(\vec{\xi}_{\bar{i}}), & \text{for } 1 \leq i \leq N-1, \\ \hat{\tilde{\mathbf{f}}}^{(EC)}(\vec{\xi}_{\bar{i}}) = \bar{f}_{(S)}(\mathbf{U}_1(\vec{\xi}_{\bar{i}}), \mathbf{U}_1(\vec{\xi}_{\bar{i}}))\hat{\tilde{\mathbf{a}}}^1(\vec{\xi}_{\bar{i}}), & \text{for } \bar{i} \in \{0, N\}, \end{cases} \tag{12}$$

$$\hat{\tilde{\vec{\mathbf{a}}}}^1(\vec{\xi}_{\bar{i}}) = \sum_{R=i+1}^{N}\sum_{L=1}^{i} 2q_{L,R}\frac{\hat{\tilde{\mathbf{a}}}^1(\vec{\xi}_L) + \hat{\tilde{\mathbf{a}}}^1(\vec{\xi}_R)}{2},$$

where $\bar{f}_{(S)}(\cdot,\cdot)$ is any two-point, entropy conservative inviscid flux that satisfies Eq. (9). In the present analysis, we use the entropy conservative flux developed in [17]. Comparing Eq. (12) with the high-order entropy stable flux in [15], we note that they are equivalent at the element faces ($\bar{i} \in \{0, N\}$) and only differ

at the interior points. Using the metric terms given by Eq.(12), the following lemma can be proven.

Lemma 1. *The inviscid flux* $\hat{\tilde{\mathbf{f}}}_l^{(EC)}$ *given by Eq.* (12) *is freestream preserving and entropy conservative, so that the following equation holds:*

$$\sum_{l=1}^{3} \mathbf{w}^\top \mathcal{P}\mathcal{P}_{\xi^l}^{-1} \Delta_{\xi^l} \hat{\tilde{\mathbf{f}}}_l^{(EC)} = \sum_{l=1}^{3} \mathbf{1}_1^\top \widehat{\mathcal{P}}_{\perp,\xi^l} \widehat{B}_{\xi^l} \hat{\mathbf{F}}_l. \tag{13}$$

Hence, $\hat{\tilde{\mathbf{f}}}_l^{(EC)}$ *given by Eq.* (12) *has the same total entropy contribution on each element as the high-order entropy consistent flux in [15].*

Proof. The proof of this lemma can be found elsewhere [6]. □

The first-order artificial dissipation fluxes $\hat{\tilde{\mathbf{f}}}_{\hat{\sigma},1}^{1(AD)}$ and $\hat{\tilde{\mathbf{f}}}_1^{1(AD)}$ for all $1 \le j \le N$ and $\vec{\xi}_i = \vec{\xi}_{ijl}$, $1 \le i \le N-1$ are defined as follows:

$$\begin{aligned}
&d\boldsymbol{\nu}_{m,n} = \tfrac{\boldsymbol{\nu}(\vec{\xi}_m) - \boldsymbol{\nu}(\vec{\xi}_n)}{\sqrt{\boldsymbol{J}(\vec{\xi}_m)\boldsymbol{J}(\vec{\xi}_n)}}, \\
&\hat{\tilde{\mathbf{f}}}_1^{1(AD)}(\vec{\xi}_i) = c_\nu^{(B)}(\mathbf{U}_1(\vec{\xi}_i), \mathbf{U}_1(\vec{\xi}_{i+1}), \hat{\tilde{\mathbf{a}}}^1(\vec{\xi}_i))\; d\boldsymbol{\nu}_{i+1,i}/(\xi_{i+1} - \xi_i)\;, \\
&\hat{\tilde{\mathbf{f}}}_{\hat{\sigma},1}^{1(AD)}(\vec{\xi}_i) = c_\nu^{(B)}(\mathbf{U}_1(\vec{\xi}_i), \mathbf{U}_1(\vec{\xi}_{i+1}), \hat{\tilde{\mathbf{a}}}^1(\vec{\xi}_i), \hat{\boldsymbol{\sigma}}_1(\vec{\xi}_i))\Big|_{\mu=\kappa=0}\; d\boldsymbol{\nu}_{i+1,i}/(\xi_{i+1} - \xi_i)\;, \\
&\hat{\tilde{\mathbf{f}}}_1^{1(AD)}(\vec{\xi}_0) = \hat{\tilde{\mathbf{f}}}_1^{1(AD)}(\vec{\xi}_N) = \hat{\tilde{\mathbf{f}}}_{\hat{\sigma},1}^{1(AD)}(\vec{\xi}_0) = \hat{\tilde{\mathbf{f}}}_{\hat{\sigma},1}^{1(AD)}(\vec{\xi}_N) = \mathbf{0},
\end{aligned} \tag{14}$$

with the identical definitions in the other computational directions. The μ, σ, and κ coefficients in $\hat{\tilde{\mathbf{f}}}_l^{1(AD)}$ are directly proportional to the artificial viscosity, $\boldsymbol{\mu}^{AD}$. At the flux points, the artificial viscosity coefficient is evaluated as the arithmetic average of the corresponding $\boldsymbol{\mu}^{AD}$ values at the neighboring solution points. The $\hat{\tilde{\mathbf{f}}}_{\hat{\sigma},l}^{1(AD)}$ flux, which is proportional to $\hat{\tilde{\boldsymbol{\sigma}}}_l$, is introduced to add the mass diffusion to guarantee the positivity of density.

5.2 Positivity of density and internal energy

We now prove that the first-order scheme given by Eq. (11) guarantees the pointwise positivity of density.

Theorem 2. *Assume that* $\hat{\tilde{\mathbf{f}}}_l^{(in)}$ *in Eq.* (11) *is the EC flux of Chandrashekar [17]. Let* $\hat{\tilde{\mathbf{a}}}_\pm^l$ *be the metric term at the "±" interface in the l-th direction. If the explicit Euler discretization in time is used in Eq.* (11)*, then this 1st–order FV scheme preserves the positivity of density under the following time step constraint:*

$$\tau < \frac{J_{ijk}}{2\sum\limits_{l=1}^{3} \frac{\mathscr{D}_l^+ + \mathscr{D}_l^-}{P_{ll}}} = \tau_\rho \tag{15}$$

with

$$\left[\lambda_c + \frac{\sigma \|\hat{\tilde{\mathbf{a}}}\|^2}{J_G \Delta\xi}\right]_l^\pm = \mathscr{D}_l^\pm \ge \mathscr{D}_{l,\min}^\pm = \frac{\rho_{l,L}^\pm}{2\rho_{l,A}^\pm} \left| \vec{\boldsymbol{V}}_A \cdot \hat{\tilde{\mathbf{a}}}_\pm^l - \mathcal{V}(\boldsymbol{u}, \boldsymbol{u}_l^\pm, \hat{\tilde{\mathbf{a}}}_\pm^l) \right|, \tag{16}$$

and the following constraint on $\sigma_l^\pm$*:*

$$\sigma_l^\pm \ge \sigma_{l,\min}^\pm = \left[\max\left(0, \frac{\rho_L}{2\rho_A} \left| \vec{\boldsymbol{V}}_A \cdot \hat{\tilde{\mathbf{a}}} - \mathcal{V}(\boldsymbol{u}, \boldsymbol{u}_l^\pm, \hat{\tilde{\mathbf{a}}}) \right| - \lambda_c \right) \frac{J_G \Delta\xi}{\|\hat{\tilde{\mathbf{a}}}\|^2} \right]_l^\pm. \tag{17}$$

Proof. The proof of this theorem is given in [6]. □

If the explicit first-order Euler scheme is used to advance the solution in time, i.e.

$$\hat{\mathbf{U}}_1^{n+1} = \hat{\mathbf{U}}_!^n + \tau \left(\hat{\mathbf{U}}_1\right)_t, \tag{18}$$

so that τ is in the interval that preserves the positivity of $\boldsymbol{\rho}^{n+1}(\vec{\xi}_{ijk})$, then the positivity of the internal energy at the time level $n+1$ at the solution point $\vec{\xi}_{ijk}$ is solely determined by the following quadratic polynomial in τ:

$$\text{IE}(\boldsymbol{u}^{n+1})\rho^{n+1} = \left(\frac{\tau}{J}\right)^2 \left(\frac{dE}{dt}\frac{d\rho}{dt} - \frac{1}{2}\left\|\frac{d\boldsymbol{m}}{dt}\right\|^2\right) + \frac{\tau}{J}\left(\boldsymbol{u}^n\right)^\top \begin{bmatrix} \frac{dE}{dt} \\ -\frac{d\boldsymbol{m}}{dt} \\ \frac{d\rho}{dt} \end{bmatrix} + \text{IE}(\boldsymbol{u}^n)\rho^n, \tag{19}$$

where $\hat{\mathbf{U}}_1^n(\vec{\xi}_{ijk}) = J\boldsymbol{u}^n$, $\mathbf{J}(\vec{\xi}_{ijk}) = J$, $\boldsymbol{\rho}^{n+1}(\vec{\xi}_{ijk}) = \rho^{n+1}$, $\left(\hat{\mathbf{U}}_1\right)_t(\vec{\xi}_{ijk}) = \left[\frac{d\rho}{dt}, \frac{d\boldsymbol{m}}{dt}, \frac{dE}{dt}\right]^\top$ and $\text{IE}(\boldsymbol{u}^n)$ is the internal energy of $\boldsymbol{u}^n$. Note that Eq. (19) holds for any spatial discretization. Using Eq. (19), we now prove the positivity of internal energy.

Theorem 3. *Let the discrete solution at the time level n be in the admissible set, so that $\boldsymbol{\rho}^n(\vec{\xi}_{ijk}), IE(\mathbf{U}_1^n(\vec{\xi}_{ijk})) > 0$ for all solution points in the domain. Then, there exists $\tau^{\min} \in (0, \tau^\rho]$, where τ^ρ is given by Eq. (15), such that for all τ: $0 < \tau < \tau^{\min}$, the 1st–order FV scheme given by Eqs. (11) and (18) preserves the positivity of internal energy, i.e., $IE(\mathbf{U}^{n+1}(\vec{\xi}_{ijk})) > 0$ at every solution point.*

Proof. The proof of this lemma can be found elsewhere [6]. □

The high-order discretization of the viscous terms may significantly increase the stiffness of the time step constraint required for temperature positivity in regions where the solution loses its regularity. To overcome this problem, we construct new conservative, discretely entropy stable limiters that bound the magnitude of the velocity and temperature gradients in troubled elements and eliminate the stiffness of the temperature positivity time step constraint. For further details on these limiters, we refer the reader to [6].

5.3 Entropy stability of the first-order scheme

The first-order scheme presented in Section 5.1 is entropy stable. Indeed, entropy stability of the first-order scheme (Eq. (11)) can be proven for the time derivative, inviscid, viscous, and artificial dissipation terms individually. Contracting Eq. (11) with entropy variables, $\mathbf{W}$, and taking into account that the mass matrices are diagonal, the time derivative term can be manipulated as $\mathbf{W}^\top \hat{\mathcal{P}} d(J\mathbf{U})/dt = \mathbf{1}^\top \hat{\mathcal{P}} d(J\mathcal{S})/dt$ (e.g., see [15]). The entropy stability of the inviscid terms follows directly from Lemma 1. The entropy stability of the high-order viscous terms and the corresponding penalties have been proven in [12, 15]. The first-order artificial dissipation terms and their penalties $\hat{\tilde{\mathbf{f}}}_l^{(ED)}$, $\hat{\tilde{\mathbf{f}}}_l^{1(AD)}$,$\hat{\tilde{\mathbf{f}}}_{\hat{\sigma},l}^{1(AD)}$, and $\hat{\mathbf{g}}_l^{1(AD)}$, are all formed by using SPSD matrices multiplied by 2-point jumps in the entropy variables and therefore are easily shown to be entropy dissipative.

6 Artificial Viscosity

The artificial viscosity, $\boldsymbol{\mu}^{AD}$, is constructed so that it ensures consistency, maintains design-order accuracy for smooth resolved solutions, and controls the amount of dissipation added in regions where the solution is under-resolved or discontinuous. Furthermore, the mass and heat viscosity coefficients of the artificial dissipation flux at each solution point are set as $\boldsymbol{\sigma}(\vec{\xi}_{ijk}) = c_\rho \boldsymbol{\mu}^{AD}(\vec{\xi}_{ijk})/\boldsymbol{\rho}(\vec{\xi}_{ijk})$, and $\boldsymbol{\kappa}(\vec{\xi}_{ijk}) = c_T \boldsymbol{\mu}^{AD}(\vec{\xi}_{ijk})$.

The scalar artificial viscosity, $\boldsymbol{\mu}^{AD}$, is used for both the high- and low-order artificial dissipation operators. Details on how the artificial viscosity coefficient is constructed are presented in [6, 24]. Herein, we only briefly outline its key elements. The artificial viscosity coefficient is constructed based on the finite element residual of the entropy equation and the physical properties of the fluid. In the k-th grid element, $\boldsymbol{\mu}^{AD}$ is defined as follows:

$$\boldsymbol{\mu}^{AD} = Sn^k \mu_{\max}^k,$$

where Sn is a sensor function ($0 \leq Sn \leq 1$) and $\mu_{\max}^k$ is the magnitude of the artificial viscosity in the k-th grid element.

To detect grid elements where the solution loses its regularity or becomes under-resolved, the sensor is constructed as a function of the finite element residual of the entropy equation, which is given by

$$Sn^k = \begin{cases} Sn_0^k, & \text{if } Sn_0^k \geq \max(0.2, \delta), \\ 0, & \text{otherwise} \end{cases} \quad Sn_0^k = \max(\mathbf{r}^k)^{\max(1, \frac{p-1}{p-1.5})}, \tag{20}$$

where p is the polynomial order and $\mathbf{r}(\vec{\xi}_{ijk})$ is a pointwise normalized entropy residual. To take into account the physics of a problem, we also augment the entropy residual-based sensor with compression and pressure gradient sensors. These sensors are introduced to identify those regions where the amount of artificial viscosity can be reduced without sacrificing the solution accuracy. We refer the reader to [6] for further details.

In each element, the upper bound of the artificial viscosity, $\mu_{\max}^k$, is set to be proportional to the maximum value of local velocity and pressure jumps between neighboring solution points [6, 24]. The result is that we minimize the amount of artificial dissipation at contact discontinuities and make $\mu_{\max}^k$ proportional to the discontinuity strength, such that the velocity and pressure jumps act as a limiter, if spurious oscillations are present in the solution.

The globally continuous artificial viscosity $\boldsymbol{\mu}_k^{AD}$ is then constructed by using the following smoothing procedure. At each element vertex, we from a unique vertex viscosity coefficient, $\mu_i^{\text{ver}} = \max_{k \in I_i} \mu_{\max}^k$, where I_i contains indices of all elements that share the i-th grid vertex. After that, the globally continuous artificial viscosity is obtained by using the tri-linear interpolation of 8 vertex viscosities, μ_i^{ver}, of the given hexahedral element.

7 High-order positivity–preserving flux-limiting scheme

7.1 Flux-limiting scheme

Herein, we generalize the 1-D high-order positivity-preserving flux-limiting method developed in [5] to three spatial dimensions. A new high-order positivity-preserving flux-limiting scheme for the 3-D Navier-Stokes equations is constructed by combining the corresponding positivity-violating high-order spectral collocation scheme (Eq. (7)) and the first-order positivity–preserving finite volume scheme given by Eq. (11) as follows:

$$\begin{aligned}
\tfrac{d\hat{\mathbf{U}}}{dt} &= \theta_f^k \left(\tfrac{d\hat{\mathbf{U}}}{dt}\right)_p + (1-\theta_f^k)\left(\tfrac{d\hat{\mathbf{U}}}{dt}\right)_1 + \left(\tfrac{d\hat{\mathbf{U}}}{dt}\right)_{AD}, \\
\left(\tfrac{d\hat{\mathbf{U}}}{dt}\right)_p &= \sum_{l=1}^{3} -\mathcal{P}_{\xi^l}^{-1}\Delta_{\xi^l}\hat{\tilde{\mathbf{f}}}_l + D_{\xi^l}\hat{\mathbf{f}}_l^{(v)} + \mathcal{P}_{\xi^l}^{-1}\hat{\mathbf{g}}_l, \\
\left(\tfrac{d\hat{\mathbf{U}}}{dt}\right)_1 &= \sum_{l=1}^{3} -\mathcal{P}_{\xi^l}^{-1}\Delta_{\xi^l}\hat{\tilde{\mathbf{f}}}_l^{(MR)} + D_{\xi^l}\hat{\mathbf{f}}_l^{(v)} + \mathcal{P}_{\xi^l}^{-1}\hat{\mathbf{g}}_l, \\
\left(\tfrac{d\hat{\mathbf{U}}}{dt}\right)_{AD} &= \sum_{l=1}^{3} \mathcal{P}_{\xi^l}^{-1}\Delta_{\xi^l}\left[(1-\theta_f^k)\hat{\tilde{\mathbf{f}}}_{\tilde{\sigma},l}^{(AD_1)} + \hat{\tilde{\mathbf{f}}}_l^{(AD_1)}\right] + D_{\xi^l}\hat{\mathbf{f}}_l^{(AD_p)} \\
&\qquad + \mathcal{P}_{\xi^l}^{-1}\left[\hat{\mathbf{g}}_l^{(AD_1)} + \hat{\mathbf{g}}_l^{(AD_p)}\right],
\end{aligned} \tag{21}$$

where the flux limiter θ_f^k ($0 \leq \theta_f^k \leq 1$) is a constant computed independently in each element and $\hat{\tilde{\mathbf{f}}}_l^{(MR)}$ is the first-order Merriam-Roe entropy dissipative flux [6, 23]. Note that the flux limiting is only applied to the inviscid terms and the mass diffusion term required for positivity of density. The term $\left(\tfrac{d\hat{\mathbf{U}}}{dt}\right)_p$ is the baseline high-order scheme with no artificial dissipation, where $\hat{\mathbf{g}}_l$ represents both the inviscid and viscous penalties.

7.2 Positivity

To prove the positivity of the high-order flux-limiting scheme (Eq. (21)), we first consider the 1st-order explicit Euler approximation of the time derivative term in Eqs. (7,11), so that on a given element

$$\hat{\mathbf{U}}_p^{n+1} = \hat{\mathbf{U}}_p^n + \tau \left(\frac{d\hat{\mathbf{U}}}{dt}\right)_p,$$
$$\hat{\mathbf{U}}_1^{n+1} = \hat{\mathbf{U}}_1^n + \tau \left(\frac{d\hat{\mathbf{U}}}{dt}\right)_1,$$

where $\hat{\mathbf{U}}_p^{n+1} = [J]\,\mathbf{U}_p^{n+1}$ and $\hat{\mathbf{U}}_1^{n+1} = [J]\,\mathbf{U}_1^{n+1}$ are pth- and first-order numerical solutions defined on the same Legendre-Gauss-Lobatto (LGL) elements with the same high-order metric terms. In the above equation, $\hat{\mathbf{U}}_1^{n+1}$ is obtained by the first-order positivity-preserving entropy stable scheme presented in Section 5.1. Therefore, at every i-th solution point of each element $\mathrm{IE}((\hat{\mathbf{U}}_1^{n+1})_i) > 0$ and $(\rho_1^{n+1})_i > 0$, where $\mathrm{IE}((\hat{\mathbf{U}}_1^{n+1})_i)$ is the internal energy associated with the 1st-order solution $(\hat{\mathbf{U}}_1^{n+1})_i$.

To combine the 1st- and pth-order schemes, we use the flux-limiting technique developed in [5], which is in fact equivalent to limiting the low- and high-order solution vectors of the conservative variables:

$$\begin{aligned}\hat{\mathbf{U}}^{n+1}(\theta_f) &= \hat{\mathbf{U}}^n + \tau\left[(1-\theta_f)\left(\frac{d\hat{\mathbf{U}}}{dt}\right)_1 + \theta_f\left(\frac{d\hat{\mathbf{U}}}{dt}\right)_p\right] \\ &= (1-\theta_f)\hat{\mathbf{U}}_1^{n+1} + \theta_f\hat{\mathbf{U}}_p^{n+1} = \hat{\mathbf{U}}_1^{n+1} + \theta_f[\hat{\mathbf{U}}_p^{n+1} - \hat{\mathbf{U}}_1^{n+1}],\end{aligned} \tag{22}$$

where the flux limiter θ_f, $0 \le \theta_f \le 1$, is a constant on a given high-order element.

At each solution point, local lower bounds of density and internal energy are defined as follows:

$$\epsilon_i^\rho = (\rho_1)_i^{n+1}\aleph, \qquad \epsilon_i^{\mathrm{IE}} = \mathrm{IE}((\hat{\mathbf{U}}_1)_i^{n+1})\aleph, \tag{23}$$

where $\aleph$, $0 < \aleph < 1$, is a function that is bounded from below by a small positive number (e.g., 10^{-8}), which approaches to its lower bound if the solution is smooth and goes to 1 if the solution loses its regularity. In the present analysis, $\aleph$ is defined as follows:

$$\aleph^k = \max(10^{-8}, L^k), \qquad L^k = Sn^k \max_i\left(\frac{|\Delta P|}{2P_A}\right), \tag{24}$$

where $0 \le Sn^k \le 1$ is the residual-based sensor given by Eq. (20) and $0 \le \max_i\left(\frac{|\Delta P|}{2P_A}\right) < 1$ is one half of the maximum relative two–point pressure jump (including jumps at the interfaces) on the kth element. Note that $0 < \epsilon_i^\rho < (\rho_1)_i^{n+1}$ and $0 < \epsilon_i^{\mathrm{IE}} < \mathrm{IE}((\hat{\mathbf{U}}_1)_i^{n+1})$ because $0 \le L^k < 1$.

Let us show that the high-order flux-limiting scheme given by Eq. (21) guarantees pointwise positivity of density and temperature.

Lemma 4. *For every i-th solution point, define a set*

$$H_i^\rho = \{\theta_f \in [0,1] \mid \rho_i^{n+1}(\theta_f) \ge \epsilon_i^\rho\}.$$

Then, the set H_i^ρ can be written as $H_i^\rho = [0, \theta_i^\rho]$ where $0 < \theta_i^\rho \le 1$. Furthermore, the following statements hold: 1) if $0 \le \theta_f < \theta_i^\rho$, then $\rho_i^{n+1}(\theta_f) > \epsilon_i^\rho$ and 2) if $\theta_i^\rho < 1$, then $\rho_i^{n+1}(\theta_i^\rho) = \epsilon_i^\rho$.

Proof. This follows directly from the fact that $\rho_i^{n+1}(\theta_f)$ given by Eq. (22) is a linear equation in the variable θ_f with $\rho_i^{n+1}(0) > \epsilon_i^\rho$. □

Lemma 5. *For every i-th solution point, define a set*

$$H_i^{IE} = \{\theta_f \in H_i^\rho \mid IE(\hat{\mathbf{U}}_i^{n+1}(\theta_f)) \ge \epsilon_i^{IE}\},$$

where $H_i^\rho = [0, \theta_i^\rho]$ is defined in Lemma 4. Then, the set H_i^{IE} can be written as $H_i^{IE} = [0, \theta_i^{IE}]$ where $0 < \theta_i^{IE} \le \theta_i^\rho$. Furthermore, the following statements hold: 1) if $0 \le \theta_f < \theta_i^{IE}$, then $IE(\hat{\mathbf{U}}_i^{n+1}(\theta_f)) > \epsilon_i^{IE}$ and 2) if $\theta_i^{IE} < \theta_i^\rho$, then $IE(\hat{\mathbf{U}}_i^{n+1}(\theta_i^{IE})) = \epsilon_i^{IE}$.

Proof. The proof of this lemma can be found elsewhere [7]. □

For a given element, we define $\theta_{\text{IE}} = \min_i\{\theta_i^{\text{IE}}\} > 0$. By construction, $\text{IE}(\hat{\mathbf{U}}_i^{n+1}(\theta_{\text{IE}})) \geq \epsilon_i^{\text{IE}}$ and $\rho(\hat{\mathbf{U}}_i^{n+1}(\theta_{\text{IE}})) \geq \epsilon_i^{\rho}$ for every solution point on the element. The solution at the $(n+1)$th time level is set equal to $\hat{\mathbf{U}}^{n+1}(\theta_{\text{IE}})$, which preserves the pointwise positivity of both density and internal energy.

7.3 Entropy stability

We now show that the high-order positivity–preserving flux-limiting semi-discrete scheme given by Eq. (21) is entropy stable. Entropy stability of the high-order viscous terms is proven in [12]. As has been discussed in Section 5.3, the first-order artificial dissipation terms are entropy dissipative. The high- and low-order inviscid entropy conservative terms must be considered together to account for the contribution of θ_f^k. Lemma 1 equates the entropy contributions of $\hat{\tilde{\mathbf{f}}}_l$ and $\hat{\tilde{\mathbf{f}}}_l^{(EC)}$ where $\hat{\tilde{\mathbf{f}}}_l^{(MR)} = \hat{\tilde{\mathbf{f}}}_l^{(EC)} - \hat{\tilde{\mathbf{f}}}_l^{(ED)}$. Therefore,

$$\sum_{l=1}^{3} \mathbf{w}^\top \mathcal{P}\mathcal{P}_{\xi^l}^{-1}\Delta_{\xi^l}\left[\theta_f^k\hat{\tilde{\mathbf{f}}}_l + (1-\theta_f^k)\hat{\tilde{\mathbf{f}}}_l^{(EC)}\right] = \mathbf{w}^\top \mathcal{P}\mathcal{P}_{\xi^l}^{-1}\Delta_{\xi^l}\hat{\tilde{\mathbf{f}}}_l \tag{25}$$

for all $0 \leq \theta_f^k \leq 1$. Thus, the $\theta_f^k\hat{\tilde{\mathbf{f}}}_l + (1-\theta_f^k)\hat{\tilde{\mathbf{f}}}_l^{(EC)}$ flux is entropy conservative, which follows directly from the fact that the high-order flux $\hat{\tilde{\mathbf{f}}}_l$ is entropy conservative, which is proven in [12, 15].

7.4 Freestream Preservation

Along with the positivity and entropy stability, the high-order positivity–preserving flux-limiting scheme given by Eq. (21) also guarantees freestream preservation. Indeed, let us consider the globally constant initial condition with the consistent Dirichlet boundary conditions and show that $\frac{d\hat{\mathbf{U}}}{dt} = \mathbf{0}_5$. Note that all artificial dissipation and viscous terms including the corresponding penalties depend directly on two-point jumps and high-order computational derivatives of the solution, respectively. Hence, all viscous terms are identically equal to zero.

We now show that all inviscid terms are also exactly equal to zero. The inviscid penalty terms are equal to zero, because of the consistency of the Merriam-Roe flux. Finally, $\hat{\tilde{\mathbf{f}}}_l$ and $\hat{\tilde{\mathbf{f}}}_l^{(EC)}$ have been proven to be freestream preserving in [15] and Lemma 1 in Section 5.3, respectively.

8 Numerical Results

To assess the accuracy, discontinuity-capturing, and positivity-preserving properties of the proposed family of high-order entropy stable spectral collocation schemes for the 3-D compressible Navier-Stokes equations, we consider standard benchmark problems with smooth and discontinuous solutions. In all numerical experiments presented herein, the 3rd-order strong stability preserving (SSP) Runge-Kutta scheme developed in [25] is used to advance the semi-discretization in time. We use the Courant-Friedrich-Levy (CFL)-type condition and the positivity time step constraints presented in Section 5.2, which guarantee positivity of density and temperature at the first Runge-Kutta stage. If the scheme fails to preserve positivity on a later Runge-Kutta stage, one can update the time step that meets the positivity constraint and repeat iterations until the positivity constraint is met for all stages. The following acronyms are used for numerical schemes in this section. The baseline high-order entropy stable spectral collocation scheme with polynomial order "#" given by Eq. (7) with $\boldsymbol{\mu}_p^{AD} = 0$ is denoted as ESSC-p#. The new positivity preserving entropy stable artificial dissipation scheme (Eq. (21)) is denoted as PPESAD-p#. The PPESAD-p# scheme with $\boldsymbol{\mu}_p^{AD}$ set to zero is denoted as PPES-p#.

8.1 3-D Viscous Shock

We validate that the proposed schemes are design-order accurate by solving the propagation of a 3-D viscous shock on a sequence of randomly perturbed nonuniform grids. The 1-D viscous shock, which possesses

	ESSC				PPESAD			
K	L_∞ error	rate	L_2 error	rate	L_∞ error	rate	L_2 error	rate
				$p=4$				
3	**1.24**	–	**4.75e-2**	–	**0.68**	–	**4.03e-2**	–
6	**0.80**	0.63	**8.50e-3**	2.48	**0.56**	0.27	**8.20e-3**	2.30
12	0.11	2.89	8.51e-4	3.32	0.11	2.37	8.51e-4	3.27
24	6.93e-3	3.96	4.96e-5	4.10	6.93e-3	3.96	4.96e-5	4.10
48	3.09e-4	4.49	1.54e-6	5.01	3.09e-4	4.49	1.54e-6	5.01
				$p=5$				
3	**3.15**	–	**3.30e-2**	–	**0.88**	–	**2.99e-2**	–
6	0.34	3.20	4.13e-3	3.00	0.34	1.36	4.13e-3	2.86
12	4.37e-2	2.97	2.49e-4	4.05	4.37e-2	2.97	2.49e-4	4.05
24	2.30e-3	4.25	7.77e-6	5.00	2.30e-3	4.25	7.77e-6	5.00
48	3.50e-5	6.04	9.99e-8	6.28	3.50e-5	6.04	9.99e-8	6.28
				$p=6$				
3	**1.27**	–	**2.11e-2**	–	**0.52**	–	**1.99e-2**	–
6	0.12	3.35	1.92e-3	3.46	0.12	2.07	1.92e-3	3.38
12	1.44e-2	3.11	7.33e-5	4.71	1.44e-2	3.11	7.33e-5	4.71
24	3.27e-4	5.46	1.20e-6	5.94	3.27e-4	5.46	1.20e-6	5.94
48	3.06e-6	6.74	7.56e-9	7.31	3.06e-6	6.74	7.56e-9	7.31

Table 1: L_∞ and L_2 errors and their convergence rates obtained with the ESSC and PPESAD schemes for $p = 4, 5, 6$ for the viscous shock problem on 3-D nonuniform grids at $t = 0.1$.

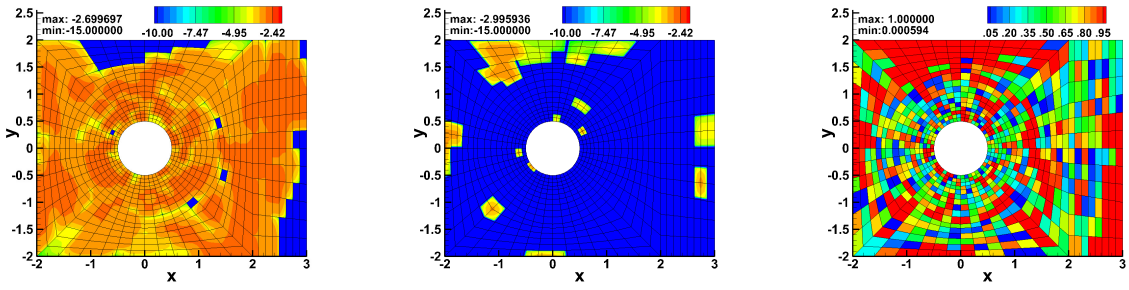

(a) (b) (c)

Figure 1: Contours of randomly generated first-order artificial viscosity (left panel), high-order artificial viscosity (middle panel), and flux limiter obtained with the PPESAD-p4 scheme for the freestream preservation problem at $t = 10$.

a smooth analytical solution at the Prandtl number $Pr = 3/4$, is rotated so that it propagates along the direction $[1, 1, 1]^\top$ and is initially centered at the origin. The Reynolds and Mach numbers are set as follows: $Re = 50$ and $Ma = 2.5$. The governing equations are integrated until $t_{\text{final}} = 0.1$. For all polynomial orders presented in Table 1, the proposed PPESAD scheme outperforms the corresponding baseline ESSC scheme in terms of accuracy on coarse grids, for which the discrete solution is under-resolved (see the results shown in bold). As the grid is refined and the viscous shock becomes fully resolved, the artificial viscosity coefficient $\boldsymbol{\mu}^{AD}$ becomes identically equal to zero and the PPESAD schemes demonstrates the same design-order error convergence as the ESSC scheme. Based on these results, we can conclude that the proposed PPESAD scheme dissipates under-resolved flow features in such a manner that reduces the error, while providing the same accuracy as the underlying ESSC scheme when the solution is sufficiently smooth and fully resolved.

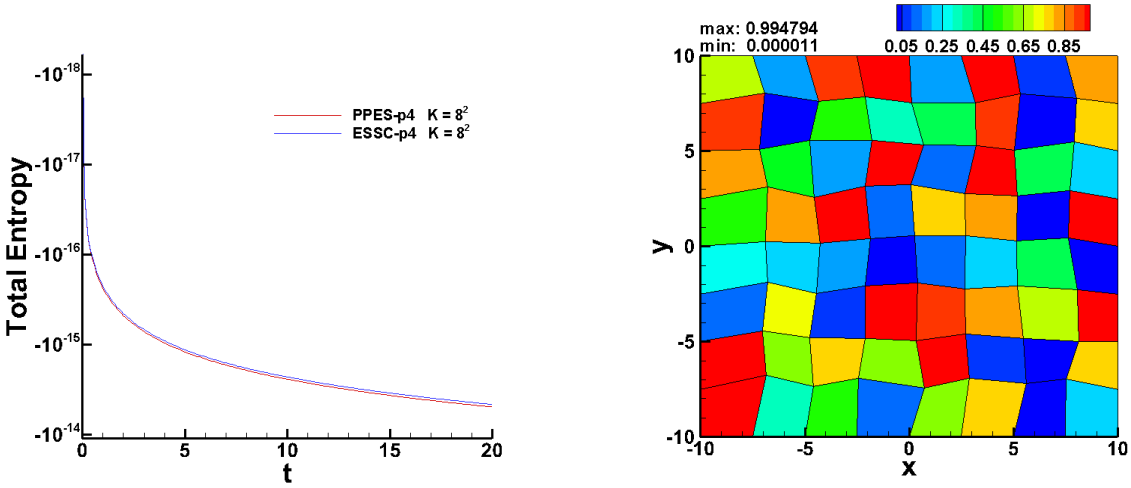

(a) (b)

Figure 2: Time histories (left panel) of the total entropy computed with the ESSC-p4 and PPES-p4 schemes and the PPES-p4 limiter coefficient (right panel) on a randomly perturbed $K = 8^2$ grid for the isentropic vortex problem.

8.2 Freestream preservation

We now corroborate our theoretical results presented in Section 7.4 and show that the new high-order positivity–preserving flux-limiting scheme given by Eq. (21) is freestream preserving on static curvilinear grids. To demonstrate this property, the 2D constant viscous flow with $\rho = 1$, $T = 1$, $\boldsymbol{V} = [\cos(10^0), \sin 10^0, 0]^\top$ at $Re = 500$, $Ma = 3.5$, and $Pr = 0.7$ is solved by using the PPESAD scheme on a 864-element genuinely curvilinear grid around a cylinder. To ensure that all terms in the high-order positivity–preserving flux-limiting scheme are turned on during the simulation, we randomly set $\boldsymbol{\mu}_p^{AD}$ and $\bar{\boldsymbol{\mu}}_1^{AD}$ to values between 0 and $1/Re$, and the flux limiter θ_f (see Section 7.1) to a value between 0 and 1 at each Runge-Kutta stage. As evident in Figure 1, all artificial dissipation and flux-limiting terms in the PPESAD scheme given by Eq. (21) are nonzero throughout the simulation. Nonetheless, the global L_2 and L_∞ errors at the final time $t_{\text{final}} = 10$ are 2.84e−15 and 1.46e−13, respectively, thus corroborating our theoretical results.

8.3 Entropy Conservation

In Lemma 1, it has been proven that the first-order positivity-preserving entropy stable scheme is entropy conservative for inviscid smooth flows, if all artificial dissipation terms are turned off. We demonstrate this property by solving the inviscid isentropic vortex flow with periodic boundary conditions at $Ma = 0.3$ on a randomly perturbed coarse grid (see Figure 2). The vortex is initially located at $(0, 0)$, propagates to the right, and returns to the origin by $t_{\text{final}} = 20$. This test problem has the exact solution (e.g., see [11]). To validate that the proposed flux-limiting scheme is entropy conservative, we randomly set the limiter value in the range between 0 and 1 at each grid element, as shown in Fig. 2. For this smooth inviscid flow with periodic boundaries, both the ESSC and PPES schemes semi-discretely conserve the total entropy in the domain. Note, however, the total entropy production obtained with the ESSC-p4 and PPES-p4 schemes with constant time step $\Delta t = 2\text{e}{-4}$ is of the order of 10^{-14} at the final time, because the 3rd-order SSP Runge-Kutta scheme used for approximating the time derivatives is not entropy conservative and violates this condition by the amount that is proportional to the truncation error of the temporal discretization.

8.4 2-D shock diffraction

The next test problem is the diffraction of a rightward moving shock over a backward-facing step at the Mach number $Ma = 200$, the Reynolds number $Re = 10^4$, and the Prandtl number $Pr = 0.75$. This

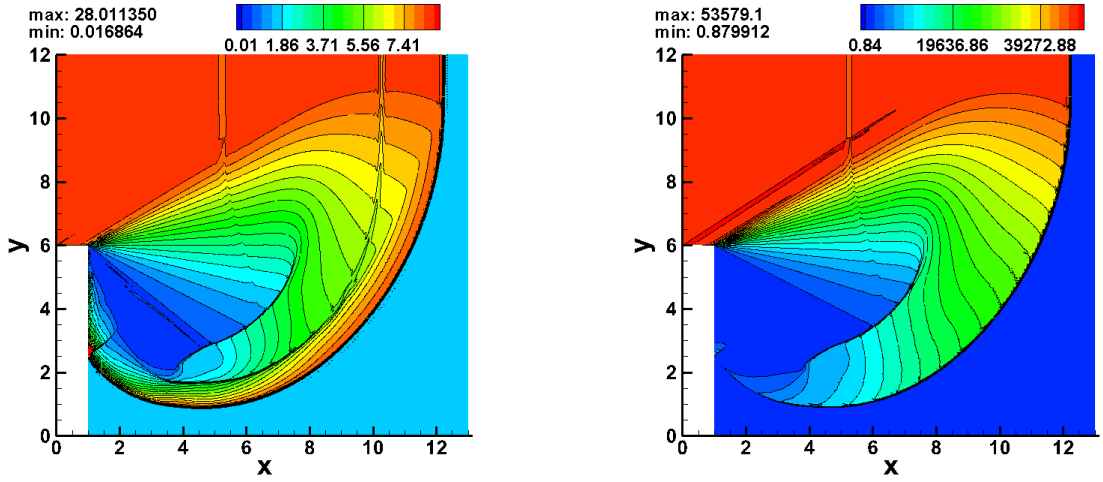

(a) (b)

Figure 3: Density and pressure contours computed with the PPESAD-p4 scheme for the viscous shock diffraction flow at $Ma = 200$.

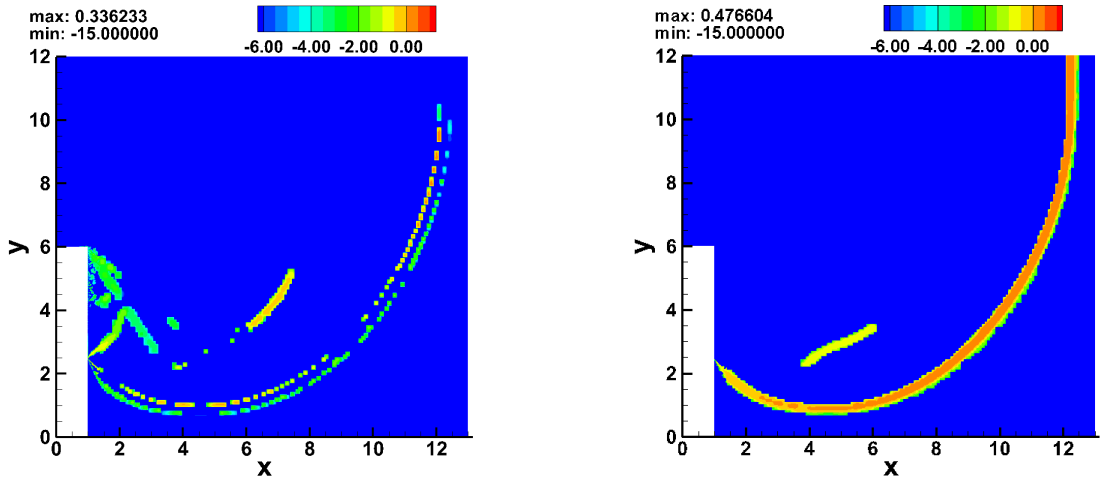

(a) (b)

Figure 4: High-order (left panel) and first-order artificial viscosities ($\log_{10}$) obtained with the PPESAD-p4 scheme for the viscous shock diffraction flow at $Ma = 200$.

is a very challenging problem that is characterized by the presence of both the strong discontinuities and regions with very low densities and pressures. If not dissipated properly, any high-order scheme can generate negative density and/or pressure values near the corner point and at the shock front. In contrast to the results presented in [1], we use the entropy stable adiabatic no-slip boundary conditions at the wall and penalize against the Blasius solution corresponding to $Ma = 200$ at the inflow boundary for solving the Navier-Stokes equations. The grid consists of 52944 elements and is clustered near the step surface, so that the normal grid spacing at the wall is 2.67×10^{-3}. The Sutherland's law is used to compute the physical viscosity coefficient.

Unlike the ESSC-p4 scheme that fails to preserve the positivity of thermodynamic variables for this viscous shock diffraction flow at $Ma = 200$, the new PPESAD-p4 scheme captures both the weak and strong shocks as well as the contact discontinuity within one grid element practically without producing any spurious oscillations, as one can see in Figure 3. Contours of the low- and high-order artificial viscosities

of the PPESAD-p4 scheme for the viscous shock diffraction flow at the final time are shown in Fig. 4. As follows from these results, the artificial viscosity coefficient is at least 3 orders of magnitude smaller at the contact discontinuity than at the shock, thus indicating that the proposed physics-based artificial dissipation method is capable of distinguishing different types of waves.

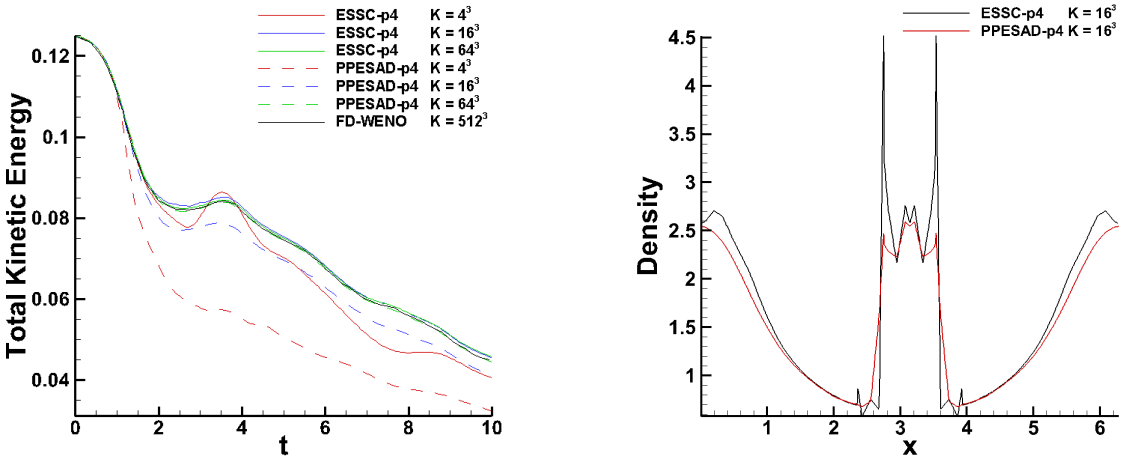

(a) (b)

Figure 5: Time histories of the total kinetic energy (left panel) and density profiles computed with the PPESAD-p4 and ESSC-p4 schemes on the 16^3 for the $Ma = 2$ TGV problem.

8.5 3-D supersonic Taylor-Green vortex flow

The last test problem is the 3-D viscous, compressible Taylor-Green vortex (TGV) flow at Mach number $Ma = 2$. This problem is considered to test how the proposed PPESAD scheme performs for under-resolved turbulent flows with strong shock waves. We adopt the TGV flow parameters used in [26]. For the TGV flow considered, the Sutherland's law is used for the physical viscosity, and the Reynolds and Prandtl numbers are 400 and 0.7, respectively. The problem is solved on the periodic cube, $0 \leq x, y, z \leq 2\pi$, with the following initial conditions: $[\rho, \boldsymbol{V}, T] = [1 + \frac{1}{16}(\cos 2x + \cos 2y)(\cos 2z + 2), \sin x \cos y \cos z, -\cos x \sin y \cos z, 0, 1]^\top$.

The comparison of kinetic energy histories obtained with the ESSC-p4 and PPESAD-p4 schemes and the hybrid 8th-order compact finite difference/ 7th-order weighted essentially nonoscillatory (WENO) scheme [26] are presented in Fig. 5a. As follows from this comparison, the kinetic energy computed using the new spectral collocation scheme on the uniform 64^3-element grid is practically identical to that of the ESSC-p4 scheme on the same grid and in an excellent agreement with that computed by the 7th-order FD-WENO scheme on the 512^3-element grid. On the 4^3 and 16^3grids, the PPESAD-p4 scheme dissipates the total kinetic energy more than the ESSC-p4 scheme. However, this does not imply that the ESSC-p4 solution is overall more accurate, which can be observed in Fig. 5b. Indeed, the ESSC-p4 solution on the 16^3 grid contains large spurious overshoots that are not present in the corresponding PPESAD-p4 solution. It should be emphasized that both solutions converge to each other as the grid is refined.

Acknowledgments

The first author acknowledges the support from Army Research Office through grant W911NF-17-0443. The second author was supported by the Department of Defense Science, Mathematics and Research for Transformation (SMART) Scholarship and the Virginia Space Grant Consortium Graduate STEM Research Fellowship.

References

[1] X. Zhang, "On positivity-preserving high order discontinuous Galerkin schemes for compressible Navier-Stokes equations," *J. Comput. Phys.*, Vol. 328, 2017, pp. 301-343.

[2] M. Svärd, "A convergent numerical scheme for the compressible Navier-Stokes equations," *SIAM J. Numer. Anal.*, Vol. 54, No. 3, 2016, pp. 1484–1506.

[3] J.-L. Guermond, M. Maier, B. Popov, I. Tomas, "Second-order invariant domain preserving approximation of the compressible Navier-Stokes equations," arXiv:2009.06022v1, 2020.

[4] J. Upperman and N. K. Yamaleev, "Positivity-preserving entropy stable schemes for the 1-D compressible Navier-Stokes equations: First-order approximation," *J. Comput. Phys.*, Vol. 466, 2022.

[5] J. Upperman and N. K. Yamaleev, "Positivity-preserving entropy stable schemes for the 1-D compressible Navier-Stokes equations: High-order flux limiting," *J. Comput. Phys.*, Vol. 466, 2022.

[6] J. Upperman and N. K. Yamaleev, "First-order positivity-preserving entropy–stable spectral collocation scheme for the 3-D compressible Navier-Stokes equations," *arXiv*:2111.03239 [math.NA], 2021.

[7] J. Upperman and N. K. Yamaleev, "High-order positivity-preserving L_2-stable spectral collocation schemes for the 3-D compressible Navier-Stokes equations," *arXiv*: 2111.08815 [math.NA], 2021.

[8] H. Brenner, "Navier-Stokes revisited," *Physica A*, Vol. 349, 2005, pp. 60–132.

[9] E. Feireisl and A. Vasseur, "New perspectives in fluid dynamics: Mathematical analysis of a model proposed by Howard Brenner," *Adv. Math. Fluid Mech.*, New directions in mathematical fluid dynamics, 2009, pp. 153–179.

[10] J.-L. Guermond and B. Popov, "Viscous regularization of the Euler equations and entropy principles," *SIAM J. Appl. Math.*, Vol. 74, 2014, pp. 284–305.

[11] N. K. Yamaleev, D. C. Del Rey Fernandez, J. Lou, and M. H. Carpenter, "Entropy stable spectral collocation schemes for the 3-D Navier-Stokes equations on dynamic unstructured grids," *J. Comput. Phys.*, Vol. 399, 2019, 108897.

[12] M. H. Carpenter, T. C. Fisher, E. J. Nielsen, and S. H. Frankel, "Entropy Stable Spectral Collocation Schemes for the Navier-Stokes Equations: Discontinuous Interfaces," *SIAM J. Sci. Comput.*, Vol. 36, No. 5, 2014, pp. B835–B867.

[13] T. C. Fisher, M. H. Carpenter, N. K. Yamaleev and S. H. Frankel, "Boundary closures for fourth-order energy stable weighted essentially non-oscillatory finite-difference schemes," *J. of Comput. Phys.*, Vol. 230, 2011, pp. 3727–3752.

[14] T. C. Fisher, M. H. Carpenter, J. Nordström, N. K. Yamaleev, and R. C. Swanson, "Discretely conservative finite-difference formulations for nonlinear conservation laws in split form: Theory and boundary conditions," *J. Comput. Phys.*, Vol. 234, 2013, pp. 353–375.

[15] M. H. Carpenter and T. C. Fisher and E. J. Nielsen and M. Parsani and M. Svärd and N. K. Yamaleev, "Entropy Stable Summation-by-Parts Formulations for Compressible Computational Fluid Dynamics," Handbook of Numerical Analysis, Vol. 17, 2016, pp. 495–524.

[16] E. Tadmor,"Entropy stability theory for difference approximations of nonlinear conservation laws and related time-dependent problems," *Acta. Numer.*, Vol. 12, 2003, pp. 451–512.

[17] P. Chandrashekar, "Kinetic energy preserving and entropy stable finite volume schemes for compressible Euler and Navier-Stokes equations," *Commun. Comput. Phys.*, Vol. 14.5, 2013, pp. 1252-1286.

[18] P. D. Thomas and C. K. Lombard, "Geometric conservation law and its application to flow computations on moving grids," *AIAA J.*, Vol. 17, 1979, pp. 1030–1037.

[19] B. Cockburn and C.-W. Shu, "The local discontinuous Galerkin method for time-dependent convection-diffusion systems, *SIAM J. Numer. Anal.*, Vol. 35, 1998, pp. 2440–2463.

[20] A. M. Rueda-Ramirez, G. Gassner, "A subcell finite volume positivity-preserving limiter for DGSEM discretizations of the Euler equations," *arXiv*:2102.06017v1 [math.NA], 2021.

[21] S. Hennemann, A. M. Rueda-Ramirez, F. Hindenlang, G. Gassner, "A provably entropy stable subcell shock capturing approach for high order split from DG for the compressible Euler equations," *J. Comput. Phys.*, Vol. 426, 2021.

[22] J. K. Upperman, "High-order Positivity-preserving L_2-stable Spectral Collocation Schemes for the 3-D compressible Navier-Stokes equations," Ph.D. thesis, Old Dominion University, 2021.

[23] M. L. Merriam, "An Entropy-Based Approach to Nonlinear Stability," NASA TM 101086, 1989.

[24] J. Upperman and N. K. Yamaleev, "Entropy stable artificial dissipation based on Brenner regularization

of the Navier-Stokes equations," *J. Comput. Phys.*, Vol. 393, 2019, pp. 74–91.

[25] C.-W. Shu, "Total-variation-diminishing time discretizations," *SIAM J. Sci. Stat. Comput.*, Vol. 9, 1988.

[26] N. Peng and Y. Yang, "Effects of the Mach number on the evolution of vortex-surface fields in compressible Taylor-Green flows," *Physical Review Fluids*, Vol. 3, No. 1, 2018.